PHYSICAL REVIEW D

PARTICLES AND FIELDS

THIRD SERIES, VOLUME 30, NUMBER 3 1 AUGUST 1984

Tests of QED at 29 GeV center-of-mass energy

D. Bender, M. Derrick, E. Fernandez, G. Gieraltowski, L. Hyman, K. Jaeger, R. Klem, P. Kooijman, S. Kooijman, J. S. Loos, F. LoPinto, B. Musgrave, L. E. Price, J. Schlereth, P. Schreiner, R. Singer, M. Valdata-Nappi,* C. Ward, J. M. Weiss, and D. E. Wood
Argonne National Laboratory, Argonne, Illinois 60439

S. Ahlen, G. Baranko, P. Baringer, D. Blockus, B. Brabson, S. Ems, G. E. Forden, R. Fries, S. W. Gray, J.-P. Guillaud, H. Neal, H. Ogren, D. Rust, and P. Smith
Indiana University, Bloomington, Indiana 47405

C. Akerlof, J. Chapman, D. Errede, N. Harnew, P. Kesten, D. I. Meyer, D. Nitz, D. Rubin, A. A. Seidl, R. Thun, T. Trinko, and M. Willutzky
University of Michigan, Ann Arbor, Michigan 48109

I. Beltrami, R. De Bonte, K. K. Gan, D. Koltick, F. Loeffler, U. Mallik, R. McIlwain, D. H. Miller, C. R. Ng, P. P. Ong, L. K. Rangan, E. I. Shibata, R. Stevens, and R. J. Wilson
Purdue University, West Lafayette, Indiana 47907

B. Cork
Lawrence Berkeley Laboratory, Berkeley, California 94720

L. Keller and J. Va'vra
Stanford Linear Accelerator Center, Stanford, California 94305
(Received 23 January 1984)

During the initial data run with the High Resolution Spectrometer (HRS) at SLAC PEP, an integrated luminosity of 19.6 pb^{-1} at a center-of-mass energy of 29 GeV was accumulated. The data on Bhabha scattering and muon pair production are compared with the predictions of QED and the standard model of electroweak interactions. The measured forward-backward charge asymmetry in the angular distribution of muon pairs is $-8.4\% \pm 4.3\%$. A comparison between the data and theoretical predictions places limits on alternative descriptions of leptons and their interactions. The existence of heavy electronlike or photonlike objects that alter the structure of the QED vertices or modify the propagator are studied in terms of the QED cutoff parameters. The Bhabha-scattering results give a lower limit on a massive photon and upper limits on the effective size of the electron of $\Lambda_+ > 121$ GeV and $\Lambda_- > 118$ GeV at the 95% confidence level. Muon pair production yields $\Lambda_+ > 172$ GeV and $\Lambda_- > 172$ GeV. If electrons have substructure, the magnitude and character of the couplings of the leptonic constituents affects the Bhabha-scattering angular distributions to such an extent that limits on the order of a TeV can be extracted on the effective interaction length of the components. For models in which the constituents interact with vector couplings of strength $g^2/4\pi \sim 1$, the energy scale Λ_{VV} for the contact interaction is measured to be greater than 1419.0 GeV at the 95% confidence level. We set limits on the production of supersymmetric scalar electrons through s-channel single-photon annihilation and t-channel inelastic scattering. Using events with two noncollinear electrons and no other charged or observed neutral particles in the final state, we see one event which is consistent with a simple supersymmetric model but which is also consistent with QED. This allows us to exclude the scalar electron to 95% confidence level in the mass range 1.8 to 14.2 GeV/c^2.

I. INTRODUCTION

The standard model of electromagnetic and weak interactions[1] includes a comprehensive theory of leptonic processes. Because the theory provides a nearly complete and precise description of such processes, it is possible to make detailed tests of the model. Electron-positron collisions are an ideal place to study such electroweak interactions. In particular, Bhabha scattering and muon pair production are, except for a small correction due to hadronic vacuum polarization,[2] calculable to any desired accuracy in terms of the standard model, the electromagnetic coupling constant, and the weak mixing angle.

The standard model is a generalization of quantum electrodynamics to include weak interactions. At energies near the masses of the vector bosons of the theory, weak effects are expected to dominate electromagnetic effects. But at SLAC PEP energies of 29 GeV in the center of mass, weak effects may be treated as corrections to lowest-order QED. The radiative corrections to lowest-order QED are of the same magnitude as the weak effects, and so experiment permits tests of both aspects of the theory.

The level of agreement between the data and the model predictions places limits on alternative descriptions of leptons and their interactions. For example, the existence of heavy electronlike or photonlike objects will alter the structure of the QED vertices, make unexpected contributions to the propagator, and introduce a non-QED momentum-transfer dependence to the cross sections. Likewise, if the electron has some finite size, a form factor will be required to describe its structure. Our measurements yield limits on the mass of new heavy objects and upper limits on the effective size of the electron and muon.

Electron-positron annihilation is also a probe of the substructure of leptons. The magnitude and character of the couplings of the leptonic constituents affects the angular distributions to such an extent that limits on the order of a TeV^{-1} can be extracted on the effective interaction length of the components. Because of the great success of the standard model, it has been further generalized into supersymmetry. The simplest such models predict that each fundamental fermion and boson will have a supersymmetric partner with identical quantum numbers except for spin. We investigate this prediction by searching for the scalar partner of the electron.

During the initial data run with the High Resolution Spectrometer (HRS), an integrated luminosity of 19.6 pb^{-1} at a center-of-mass energy of 29 GeV was accumulated. We have made measurements of Bhabha scattering and muon pair production using this data set. The HRS has since accumulated a total integrated luminosity about six times as large. Analysis of this larger data set will be reported at a later date.

II. DETECTOR

The HRS, shown in Fig. 1, is a general-purpose spectrometer which measures both charged particles and electromagnetic energy over 90% of the solid angle. The

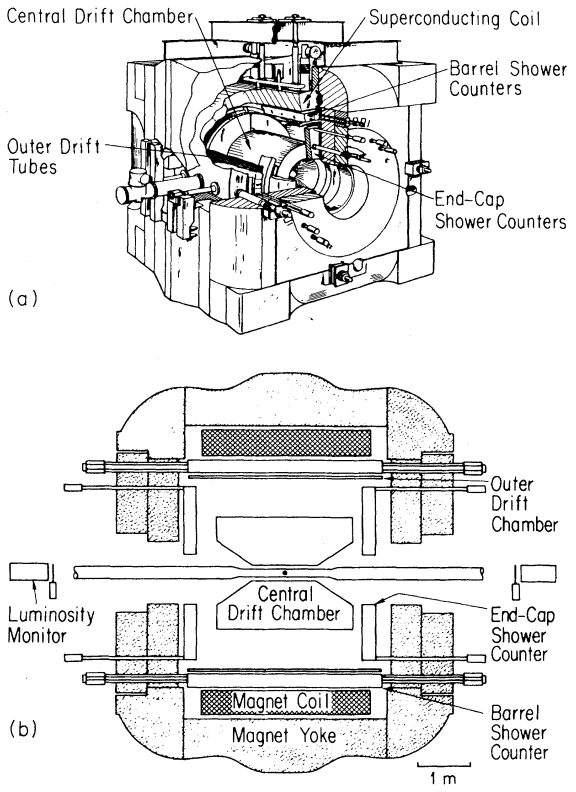

FIG. 1. The High Resolution Spectrometer (HRS). (a) Perspective view. (b) Cross-sectional view.

detection elements are in a 1.62-T magnetic field with a cylindrical volume of 4.45 m in diameter by 3.88 m long. The field uniformity is such that $\Delta B/B_0$ is less than 1.5% over the main tracking region, where B_0 is the central field value.

During the first running period, the detector elements of the HRS consisted of a central drift chamber, an outer drift-chamber system, a barrel shower counter, and an end-cap shower-counter system.

The central drift chamber tracks charged particles using 15 cylindrical layers of drift cells.[3] In seven of the layers the wires are oriented axially, and in the remaining eight layers they are at a stereo angle of ± 60 mr. The innermost layer is at a radial distance of 21 cm from the beam line, and the outermost layer is at 103 cm. The outer drift chamber was designed to significantly improve the spectrometer momentum resolution for charged tracks.[4] It consists of two layers of drift tubes comprising a cylinder 1.89 m in radius and 3.5 m in length. The tubes are 2.58 cm in diameter. The drift-chamber systems have a total of 3344 cells with a measured spatial resolution of 200 μm. The predicted momentum resolution of the HRS including and excluding the outer-drift-chamber information is shown in Fig. 2.

As seen in Fig. 2, the high-momentum tracks have a resolution which is dominated by measuring error whereas multiple scattering dominates at low momentum. To minimize the latter effect the storage ring vacuum pipe was made of 0.14-cm-thick beryllium with a 0.025-cm aluminum coating to absorb synchrotron photons. The

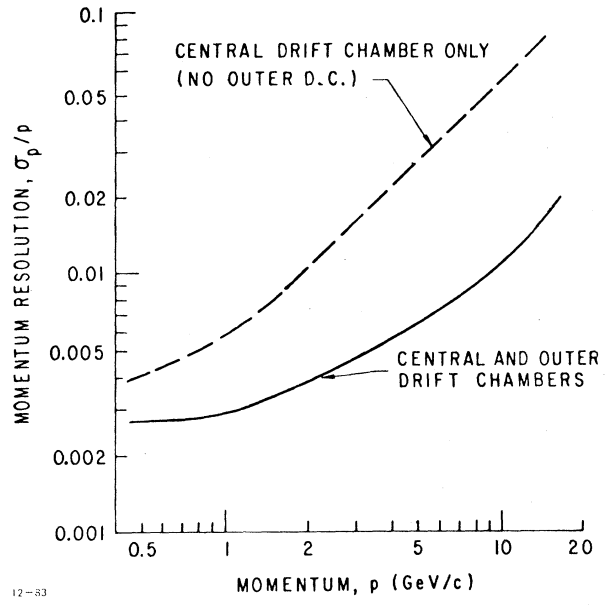

FIG. 2. Calculated momentum resolution with and without the outer drift-chamber system.

chamber support structures were also designed to minimize multiple scattering of the outgoing particles. The result is that a typical track traverses 0.02 radiation lengths of material. This unique combination of high magnetic field, extensive tracking range, low multiple scattering, and precise spatial measurement, yields a momentum resolution of

$$\frac{\sigma_p}{p} = 1.0\times 10^{-3} p \quad (p \text{ in GeV}/c)$$

for $|\cos\theta| < 0.7$ and $p > 5$ GeV/c. The charge of a 14.5-GeV/c particle is unambiguously identified for $|\cos\theta| < 0.91$.

The momentum accuracy of the HRS can be checked using Bhabha-scattered events since they provide a sample of particles of known momentum. Figure 3 shows the momentum distribution of Bhabha-scattering electrons including points measured in the outer drift chamber and with the tracks constrained to the known vertex. The width of the distribution is due predominantly to measuring error. The contributions from the beam-energy spread and radiative effects are negligible.

The barrel shower-counter system is used to identify and measure the location of electromagnetic energy and determines the time of flight for particles that traverse the spectrometer. The barrel system consists of 40 modules arranged as the staves of a barrel inside the magnet cryostate with an inner radius of 194.3 cm. The active length of the system is 304.8 cm and it covers 62% of the solid angle. Each module contains three distinct detector segments. The front section consists of a $2X_0$ layer of lead followed by a 1.27-cm-thick layer of scintillator followed by $1X_0$ of lead and another 1.27-cm-thick layer of scintillator. This section of each module is read out with a phototube at each end and provides both time-of-flight information and shower information. The second section of the module is a layer of proportional tubes, made from 3.66-m-long aluminum extrusions, each with 14 cells, 1.9 cm square. The chambers are instrumented for current division measurements and are able to locate a shower position along the wire to an accuracy of ± 2 cm. The last section of the module consists of alternating layers of $1X_0$ of lead and 0.79 cm of scintillator and is read out with a single phototube at each end of the module. For normal incidence, the total number of radiation lengths in the system is $11X_0$.

The time-of-flight measurement for minimum-ionizing particles has a RMS error of 360 psec. The error for electrons is 160 psec which is a measure of the stability of the system. The energy resolution for showering particles was measured in a test beam to be $\sigma_E/E = 0.16/\sqrt{E}$ (E in GeV) for energies less than 5 GeV. As the energy increases beyond 5 GeV, a significant fraction of the shower leaks out the back of the counter, the resolution is degraded and levels off at about $\sigma_E/E = 7\%$. Monte Carlo simulations indicate that 30% of the energy in a 14.5-GeV shower is lost because of leakage. Figure 4(a) shows the energy distribution of minimum-ionizing particles. The peak for minimum-ionizing particles is at 200 MeV. Figure 4(b) shows the measured energy distribution of 14.5-GeV Bhabha-scattering positrons and electrons. The distribution has a full width at half maximum of 3.5 GeV

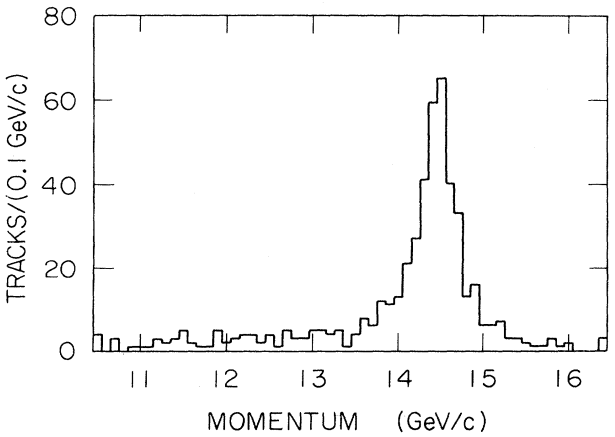

FIG. 3. The observed momentum distribution of fully constrained Bhabha-scattering events.

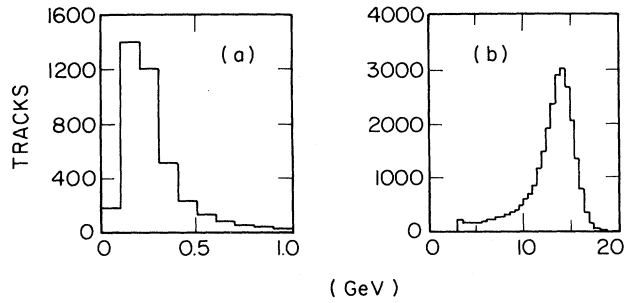

FIG. 4. The observed energy distribution in the barrel shower-counter system for (a) minimum-ionizing tracks and (b) Bhabha-scattered tracks.

because tracks hitting near cracks and edges have not been excluded.

The end-cap shower counters provide electromagnetic calorimetry and time-of-flight information over 27% of the solid angle. The end caps cover the ends of the solenoid at a distance of $+1.48$ and -1.65 m from the midplane of the detector. The system contains 40 pie-shaped modules, each of which uses a wave shifter to transmit scintillation light through a light pipe to a single photomultiplier tube. The modules are $8.7X_0$ thick, consisting of eight layers of lead and scintillator. A single $1.7X_0$-thick sheet of lead makes up the first layer of the counters, followed immediately by a single layer of proportional wire chambers, which have characteristics identical to those in the barrel shower-counter system. The energy resolution for showers with $E<5$ GeV is $\sigma_E/E=0.20/\sqrt{E}$. The energy distributions for minimum-ionizing particles and Bhabha-scattered electrons and positrons are shown in Figs. 5(a) and 5(b).

The recorded events were required to satisfy at least one of several triggers. A primary trigger resulted from hits in at least 12 of the 15 layers of the inner drift chamber, or at least four of the innermost eight layers in addition to a hit in the end caps. A secondary trigger required that the curvature processor identify two tracks with momenta greater than 3 GeV/c and be in time with the beam crossing. Small angle tracks had to be accompanied by a hit in the end cap. The high efficiency ($>99\%$) of the central drift chamber guarantees a uniform acceptance by the charged trigger for events in which both tracks exit the chamber beyond the seventh drift-chamber layer ($|\cos\theta|<0.92$).

Cracks in the shower counter time-of-flight system reduce the efficiency in well-defined regions. Triggers having only two found tracks required at least one barrel counter to be in time with the beam crossing to within 30 nsec. Two neutral triggers were also used. The first required that more than 4.8 GeV be deposited in the shower counters. The threshold for the second neutral trigger was set at 2.4 GeV, but at least one charged track was required in addition. The data were written to magnetic tape by a VAX 11/780 computer at a rate of 2 to 3 Hz. The detector dead time was typically 12%. During this first run 16×10^6 triggers were recorded.

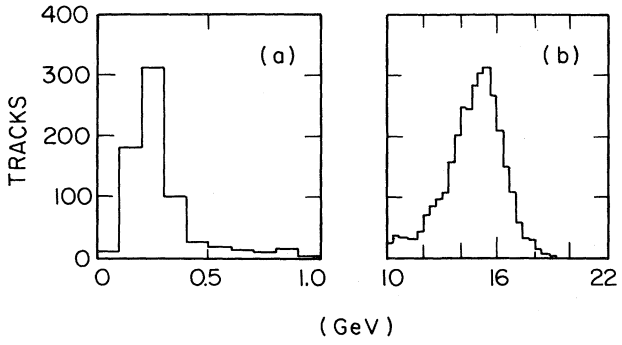

FIG. 5. The observed energy distribution in the end-cap shower-counter system (a) minimum-ionizing tracks. (b) Bhabha-scattered tracks.

III. EVENT SELECTION

For an event to be accepted as a muon pair or a Bhabha candidate it had to satisfy all of the following conditions. (1) The event must contain two and only two oppositely charged particles. Tracks with momenta less than 100 MeV/c were not counted. (2) The momentum of each of the particles was greater than 7.25 GeV/c. This cut was made to eliminate beam-gas scattering since the observed momentum is always less than or equal to the energy of a single beam. (3) The acollinearity of the two high-momentum particles was less than 25°. (4) The distance of closest approach of the tracks to the interaction point was less than 1.0 cm radially and 9.0 cm along the beam direction. (5) Each high-momentum track was associated with a signal from an electromagnetic shower counter indicating a flight time within 15.0 nsec of the beam-crossing time. (6) The flight time difference between the two particles must be less than 6 nsec if the particle was in the barrel shower-counter region or 8 nsec if it was in the end-cap shower-counter region.

A particle was classified as a muon or a minimum-ionizing particle if the shower-counter energy was less than 1.0 GeV. If the shower energy was greater than 40% of the particle's momentum, then the particle was considered to be an electron or positron. An event was included in the muon pair or Bhabha samples only when both particles were identified as muons or else as electrons. The vertex and timing requirements were designed to reject cosmic rays. The distribution of the difference in

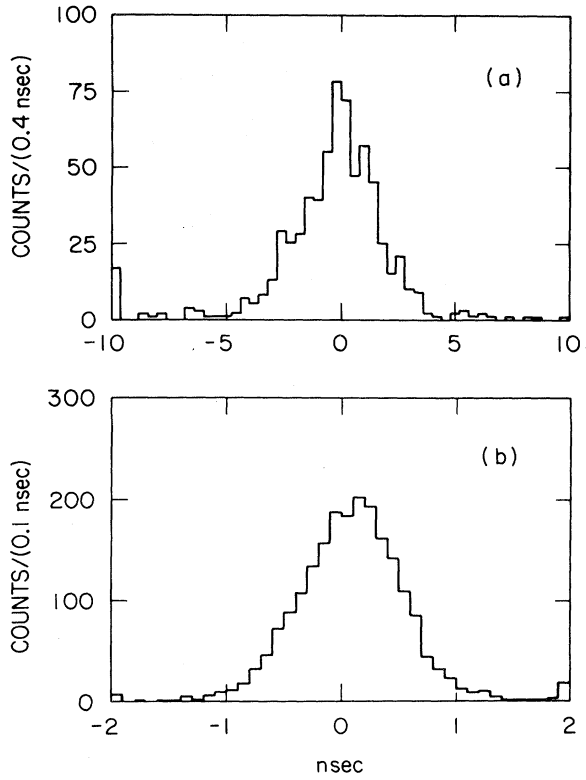

FIG. 6. The observed time-of-flight residuals in (a) the end-cap system and (b) the barrel system.

time of flight for the two particles is shown in Fig. 6. The cosmic-ray signal is well separated from the dilepton signal.

Geometric cuts were placed on the candidates so that gaps in the detector acceptance were avoided. The barrel shower counters cover the polar angle with uniform efficiency for $|\cos\theta| < 0.55$. The end-cap shower-counter acceptance is $0.85 > |\cos\theta| > 0.75$. The aluminum wall of the barrel modules produces a periodic gap in the azimuthal acceptance every 9°. The modules have an effective width of 8.0° separated by a 1.0° gap. Figure 7 shows the energy deposited as a function of azimuthal angle, modulo 9°. There are also gaps in the end-cap acceptance along the radial strips that separate the pie sections of the scintillators. The width of the gaps is 1.0 cm and occur at 18° intervals.

When the polar angle of the track is such that $|\cos\theta| > 0.91$, the track leaves the inner drift chamber after having traversed fewer than eight layers. The track-finding efficiency deteriorates for this region and there is some ambiguity as to the charge of the particle. The tracking efficiency versus polar angle was estimated using a Monte Carlo program. The result is shown in Fig. 8.

These geometric cuts ensure that events were accepted only within regions of the detector where the detection efficiency is uniform. The resulting data sample consists of 8915 Bhabha events and 811 muon pairs detected in the end caps.

There is excellent separation between events with showering electrons and minimum-ionizing muons, with an estimated contamination by Bhabha events in the muon sample of less than 0.1%. However, other annihilation phenomena have similar final-state topologies which can feed into the data samples. The largest contribution comes from τ pair production with about 4% of the pairs generating two electrons in the final state and about 25% generating a pair of minimum-ionizing particles. Of the pairs produced, only a fraction survive the momentum and acollinearity cuts. Monte Carlo studies find that the τ contamination of the Bhabha sample is negligible, being less than 0.03%. The effect on the muon sample is found

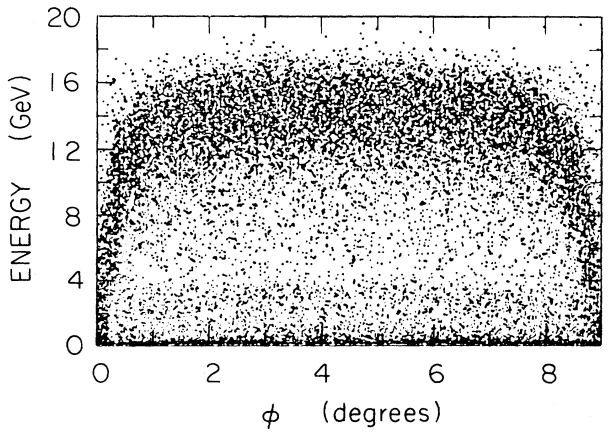

FIG. 7. The shower-counter energy distribution vs azimuth angle, modulo 9°.

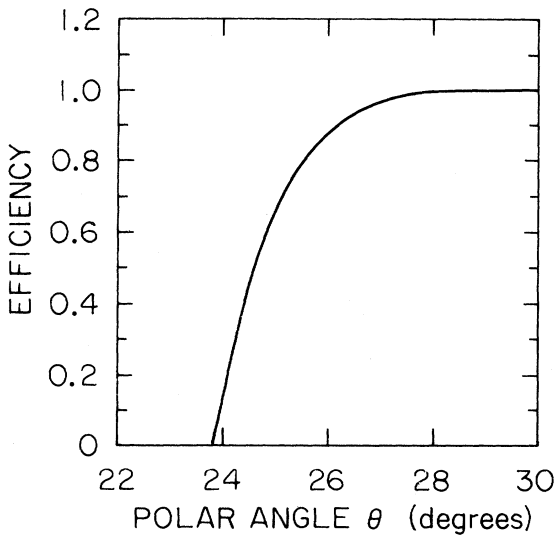

FIG. 8. The tracking efficiency as a function of the polar angle.

to be 1.1%, but because the angular distribution of the τ pairs is similar to that of the muon pairs its effect on the measurement of the muon asymmetry is negligible. Two-photon annihilations can also yield a final state with two electrons or two minimum-ionizing particles when a small angle pair escapes detection. Again, such topologies will rarely survive the momentum and acollinearity cuts and generate a background to the muon sample of less than 0.1%.

Radiative effects will cause the loss of events. An event with a final-state photon that converts in the beam pipe or detector material can cause the multiplicity of the event to be considered greater than two. Using the EGS program,[5] this effect was found to cause a 0.3% loss of the sample. A radiative photon which does not convert but which hits in a shower module near a muon will cause the muon to be misidentified. Using the Monte Carlo program, about 5% of the muons are misidentified in this way. The data is fully corrected for this effect.

Finally, cosmic-ray events can feed into the muon sample. By increasing the time of flight and vertex cuts, it is estimated that less than 0.6% of the muon sample are cosmic rays.

IV. MONTE CARLO SIMULATIONS

In this experiment, the selection of Bhabha and muon pairs is based on the momenta of the outgoing leptons and only indirectly on the energy of any radiated photon. The event generators for both Bhabha scattering and muon pair production are those of Berends, Kleiss, and Jadach.[6] The generators are structurally identical. The differential cross section for these processes is given by

$$\frac{d\sigma}{d\Omega} = \frac{d\sigma_0}{d\Omega}(1+\delta_a+\delta_b+\delta_\tau+\delta_h+\delta_w) ,$$

where $d\sigma_0/d\Omega$ is the lowest-order QED cross section. δ_a contains all purely QED radiative effects including vacuum polarization due to the electron and muon loops and soft bremsstrahlung. The effect of hard bremsstrahlung is

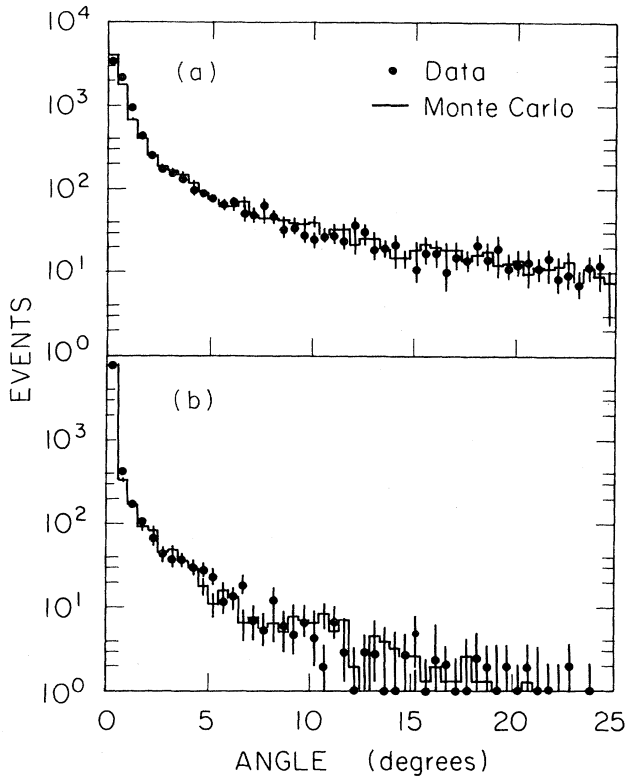

FIG. 9. (a) The acollinearity-angle distribution for Bhabha scattering. (b) The acoplanarity-angle distribution for Bhabha scattering.

contained in δ_b. δ_τ is the τ vacuum polarization and δ_h is the hadronic vacuum polarization. Weak effects are contained in δ_w. The Monte Carlo is used to generate elastic events for both Bhabha scattering and muon pair according to the full distributions.

The Monte Carlo event generator produces final-state four-vectors for the lepton pair and radiated photon. The response of the detector to each final state is determined by applying the known-detector-response characteristics to each generated final-state particle. Effects of multiple scattering in the structural elements as well as the chamber gas are included. The program generated drift-chamber and shower-counter information with drift times and pulse heights smeared to reflect the finite resolution of the detector. The result is stored as a raw event record identical in form to a real data record. The event is then reconstructed from the raw simulated data by essentially the same algorithm that is used to reconstruct the real data. The same analysis and acceptance criteria are applied to both the real data and the Monte Carlo data. We compare the theoretical and the measured distributions that result from the analysis in Figs. 9(a) and 9(b).

V. COMPARISON OF RESULTS WITH THE STANDARD MODEL (Ref. 7)

A. Total muon-pair cross section

The integrated luminosity for the sample is measured by counting the number of Bhabha events in which both tracks are detected in the barrel shower counter system, $|\cos\theta| < 0.55$. The Monte Carlo gives the total cross section corresponding to the defined acceptance. The cross section for muon pairs with the same acceptance is

$$\sigma(e^+e^-\to\mu^+\mu^-)=0.0353\pm0.0015 \text{ nb} .$$

The QED prediction calculated for identical acceptance is 0.0352 ± 0.0008 nb. The pointlike cross section for muon pair production yields a cross section of

$$\sigma_{\text{point}}(e^+e^-\to\mu^+\mu^-)=0.0365 \text{ nb}$$

for the same acceptance. The ratio of the measured cross section to the pointlike cross section is 0.968 ± 0.04. Although the radiative effects are not small (in fact about 5% of the muon-pair events are lost because a hard photon hits a shower-counter module near a muon track), their net effect after cuts is to yield a cross section very near the pointlike result.

The total muon cross section can be used to set limits on the QED cutoff parameter. The cutoff would alter the cross section in the following way:

$$\sigma=\sigma_{\text{QED}}\left[1\pm\frac{2s}{\Lambda_\pm^2}\right] .$$

Using the measured and predicted values for the cross section gives limits of $\Lambda_+ > 172$ GeV and $\Lambda_- > 172$ GeV, at 95% confidence level. A comparison with other experiments is shown in Table I.

TABLE I. The QED cutoff parameter found from muon-pair production.

Experiment	Λ_+ (GeV)	Λ_- (GeV)
HRS	172	172
PLUTO[a]	267	126
TASSO[b]	150	251
MARK J[c]	355	209
CELLO[d]	186	101

[a]Ch. Berger *et al.*, Z. Phys. C **21**, 53 (1983).
[b]R. Brandelik *et al.*, Phys. Lett. **117B**, 365 (1982).
[c]D. Adeva *et al.*, MIT Laboratory for Nuclear Science Report No. 131, 1983 (unpublished).
[d]H. J. Behrend *et al.*, Z. Phys. C **14**, 283 (1982).

B. Bhabha scattering

The angular distribution for Bhabha-scattered positrons is shown in Fig. 10. The data are corrected for radiative effects and detector acceptance. Deviations from pure QED are parametrized in terms of $\delta(\cos\theta)$, where

$$\delta_{\text{meas}}(\cos\theta)=\left[\frac{d\sigma_{\text{meas}}}{d\Omega}-\frac{d\sigma_{\text{QED}}}{d\Omega}\right]\left[\frac{d\sigma_0}{d\Omega}\right]^{-1} .$$

$d\sigma_0/d\Omega$ is the lowest-order QED differential cross section. $d\sigma_{\text{QED}}/d\Omega$ represents pure QED to order α^3 and includes the effects of hadronic vacuum polarization:[8]

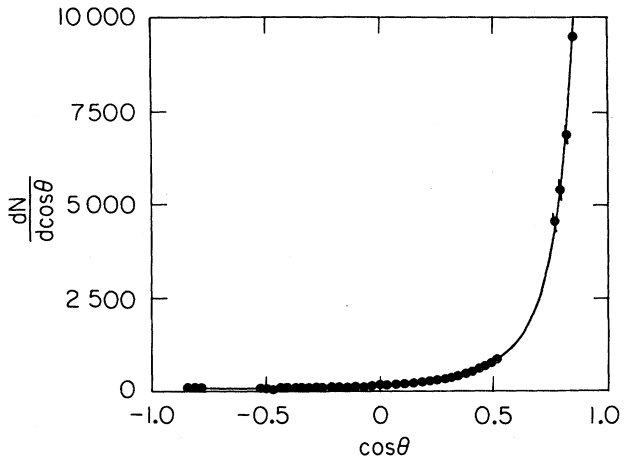

FIG. 10. The angular distribution of Bhabha-scattering positrons.

$$\frac{d\sigma_{\rm QED}}{d\Omega}=\frac{d\sigma_0}{d\Omega}(1+\delta_a+\delta_b+\delta_h+\delta_\tau)\ .$$

In practice $d\sigma_{\rm QED}/d\Omega$ is calculated by Monte Carlo generation. A luminosity measurement independent of the Bhabha-scattered events is unavailable making the overall normalization unknown. Then $\delta_{\rm meas}$ is defined as follows:

$$\delta_{\rm meas}(i)=\frac{N_d^i/N_d-N_{\rm MC}^i/N_{\rm MC}}{(d\sigma_0^i/\sigma_0)}\ .$$

N_d^i and $N_{\rm MC}^i$ are the number of events in the ith $\cos\theta$ bin for the observed and the generated distributions. N_d and $N_{\rm MC}$ are the total numbers of events. The denominator contains the lowest-order differential cross section integrated over the width of the bin and normalized by the total cross section. $\delta_{\rm meas}(\cos\theta)$ is shown in Fig. 11.

Deviations from standard QED may exist in the form of a heavy electronlike object or heavy photon which will modify the lepton-photon vertex or the photon propagator. There is also the possibility that the electron is not pointlike but that it has some finite charge distribution.

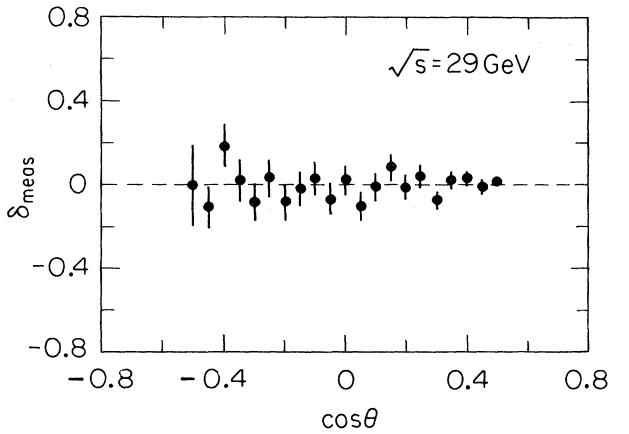

FIG. 11. The normalized difference between the measured and predicted Bhabha-scattering distributions vs $\cos\theta$.

TABLE II. The QED cutoff parameter found from Bhabha scattering.

Experiment	Λ_+ (GeV)	Λ_- (GeV)
HRS	121	118
CELLO[a]	83	155
JADE[b]	178	200
MARK J[c]	173	177
PLUTO[d]	80	234
TASSO[e]	136	281

[a]H. J. Behrend *et al.*, Phys. Lett. **103B**, 148 (1981).
[b]W. Bartel *et al.*, Z. Phys. C **19**, 197 (1983).
[c]D. Adeva *et al.*, MIT Laboratory for Nuclear Science Report No. 131, 1983 (unpublished).
[d]Ch. Berger, *et al.*, Z. Phys. C **4**, 269 (1980).
[e]R. Brandelik, Phys. Lett. **110B**, 173 (1982).

These effects will alter the angular distribution of Bhabha scattering and are characterized by the QED cutoff parameter $\Lambda_\pm$,[9]

$$\pm\delta_c(s)=\frac{3s}{\Lambda_\pm^2}\frac{1-\cos^2\theta}{3+\cos^2\theta}$$

such that

$$\frac{d\sigma}{d\Omega}=\frac{d\sigma_0}{d\Omega}[1\pm\delta_c(s)]\ .$$

The QED cutoff parameters are determined by a comparison of $\delta_{\rm meas}(\cos\theta)$ with the theoretical deviation expected for an electron of finite size. A χ^2 is defined where

$$\chi^2=\sum_{i=1}^{N}\left[\frac{\delta_{\rm meas}^i-\delta(\cos\theta_i,\Lambda)}{\sigma_{\rm meas}^i}\right]^2\ .$$

Then χ^2 is a function of Λ. If $\delta(\cos\theta,\Lambda)$ is a good fit to the data, then 95% of all experiments will measure $\chi^2(\Lambda)<\chi^2_{95}$, where χ^2_{95} is determined by the number of degrees of freedom N. The value of Λ for which $\chi^2(\Lambda)=\chi^2_{95}$ is the 95%-confidence-level cutoff parameter. The results of the fit are given for $\pm\delta_c$ in Table II.

C. Tests of leptonic substructure

The existence of at least three generations of quarks and leptons has led to speculation that the observed fermions are composites of more fundamental particles called preons. Experimentally there is no indication that the electron has structure. Lower limits for cutoff parameters are in the 100—200-GeV range, corresponding to an electron size of less than 10^{-16} cm. Therefore, if the electron is a composite particle its constituents are strongly bound, giving the electron the observed pointlike quality at experimentally accessible energies.

Bhabha scattering is a useful probe of the structure of the electron. High-energy collisions of electrons and positrons will involve the direct interaction exchange of the electron constituents. There will be interference between the QED amplitude and the amplitude due to the interaction of the preons. The observed distribution will reflect the contribution of the strong interaction of the preons

TABLE III. The preon-mass-scale lower limits obtained from Bhabha-scattering results in this experiment.

Couplings	Λ_+ (GeV)	Λ_- (GeV)
Axial-vector	810	1061
Vector	1419	1375
Right- (left-) handed	638	509

and imply a limit for the effective interaction length or mass of the constituents of the electron.

Eichten, Lane, and Peskin[10] have calculated the cross section for the scattering of such composite electrons and positrons. The energy scale for the preon-binding interaction is Λ_P and if it is greater than the energy at which electroweak symmetry is broken, then $\Lambda_P > \Lambda_{EW} \sim 1$ TeV. At energies small with respect to Λ_P, the exchange of the constituents leads to a four-fermion contact interaction with strength $g^2/\Lambda_P{}^2$, the coupling is necessarily strong and $g^2/4\pi$ is of order 1. The effect of the constituents on the cross section is

$$\frac{d\sigma_0}{d\Omega}\delta_P = \frac{\alpha}{8s\Lambda^2}\left[8\left[\frac{s}{t}\right]^2 t\eta_{LR} + 2s\eta_{LR}(1-\cos\theta)^2 + \left[1+\frac{s}{t}\right]2s(\eta_{RR}+\eta_{LL})\right],$$

so that

$$\frac{d\sigma}{d\Omega} = \frac{d\sigma_0}{d\Omega}[1+\delta_P(\Lambda)] .$$

If only the left-handed component of the electron is composite, then $\eta_{LL} = \pm 1$ and $\eta_{RR} = \eta_{RL} = 0$. If both left- and right-handed helicity states of the electron are composite, then $|\eta_{RL}| = 1$. The interference term is largest if both helicity components are composite. At PEP energies where weak effects are small, left- (LL) and right- (RR) handed models give the same limit for Λ_P. If $\eta_{LL} = \eta_{RR} = \eta_{RL} = \eta_{LR} = \pm 1$ there is vector (VV) coupling. Axial-vector (AA) coupling results when $\eta_{RR} = \eta_{LL} = -\eta_{RL} = -\eta_{LR} = \pm 1$. The data yield lower limits for Λ_P for models with purely left-handed, right-handed, vector, or axial-vector currents. The limit for Λ_P is nearly an order of magnitude higher (depending on the constituent coupling) than the limit $\Lambda_\pm$ described above. Results at 95% confidence level are shown in Table III.

D. Weak-interaction parameters

The correction to pure QED due to weak interactions is parametrized in terms of the axial-vector and vector couplings and the mass of the Z^0, or alternatively in terms of the weak mixing angle in the standard model. The parameters are measured by fitting the expected electroweak distribution to the radiatively corrected data.[11] Sensitivity to the axial-vector coupling comes from the muon data. The forward-backward charge asymmetry is directly proportional to g_A when $g_V \ll 1$. The ratio of Bhabha events to muon events yields information on the vector coupling. The Bhabha and muon-pair data are therefore treated simultaneously.

The maximum-likelihood method is used to calculate the values for the weak-interaction parameters that best fit the data. The likelihood function L, for a given set of weak parameters g_V and g_A, is

$$L = \prod_{i=1}^{N_{\text{events}}} P(g_V, g_A, \cos\theta_i)$$

where $P(g_V, g_A, \cos\theta)$ is the normalized distribution function for events at $\cos\theta$ in a theory with weak couplings g_V and g_A. The distribution $P(g_V, g_A, \cos\theta)$ is the sum of the differential cross sections for muon-pair production and for Bhabha scattering including weak and α^3 radiative effects after corrections for detector acceptance. The likelihood function is the probability of measuring the observed distribution of events. We have

$$P(g_V, g_A, \cos\theta_i) = \frac{1}{N(g_V, g_A)}\left[\frac{d\sigma_{ee}}{d\cos\theta}(g_V, g_A, \cos\theta_i) + \frac{d\sigma_{\mu\mu}}{d\cos\theta}(g_V, g_A, \cos\theta_i)\right]$$

and

$$\frac{d\sigma}{d\cos\theta} = \frac{d\sigma_0}{d\cos\theta}(1+\delta_w+\delta_{\text{rad}}+\delta_{\text{acc}}) .$$

δ_w contains the weak effects and is a function of g_V and g_A. Radiative corrections are included in δ_{rad}. δ_{acc} is the correction for detector geometric acceptance and efficiency. $P(g_V, g_A, \cos\theta)$ is determined for each Bhabha and muon-pair event at $\cos\theta_i$ by calculating $d\sigma_{ee}/d\cos\theta_i$ or $d\sigma_{\mu\mu}/d\cos\theta_i$. The differential cross sections, and therefore P, can alternatively be defined as a function of θ_w. The fit then yields a best value for the weak mixing angle.

The simultaneous fit to the Bhabha and muon-pair data determines the vector coupling and requires that the systematic bias in the efficiency for detecting the final states be small compared to the size of the weak correction to the total cross sections. Therefore, we choose to perform the simultaneous fit exclusively for the events detected by the barrel shower counter. The measured vector coupling can then be used in an independent fit of the muon pairs detected in both the barrel and end-cap counters. The final value of the axial-vector coupling constant is thus based on a fit to the full sample of muon-pair events. The simultaneous fit gives $g_V{}^2 = 0.00 \pm 0.18$ and $g_A{}^2 = 0.25 \pm 0.21$ with the mass of the Z^0 fixed at 88.4 GeV (Ref. 12). The fit for θ_W yields $\sin^2\theta_W = 0.17 \pm 0.20$.

In order to fit the full sample of muon data we define the normalized probability

$$P(g_A, \cos\theta) = \frac{1}{N(g_A)}\left[\frac{d\sigma_{\mu\mu}}{d\cos\theta}(g_A, \cos\theta)\right],$$

and maximize the likelihood function with respect to g_A having fixed g_V at the value determined by the simultaneous fit with $M_Z = 88.4$ GeV. Note that the shape of the muon-pair differential cross section is sensitive to g_A and not to g_V. The result of the independent fit to the complete sample of muon data (barrel and end-cap counters) is $g_A{}^2 = 0.33 \pm 0.17$. The fit yields a muon-pair forward-backward charge asymmetry over the full solid angle of

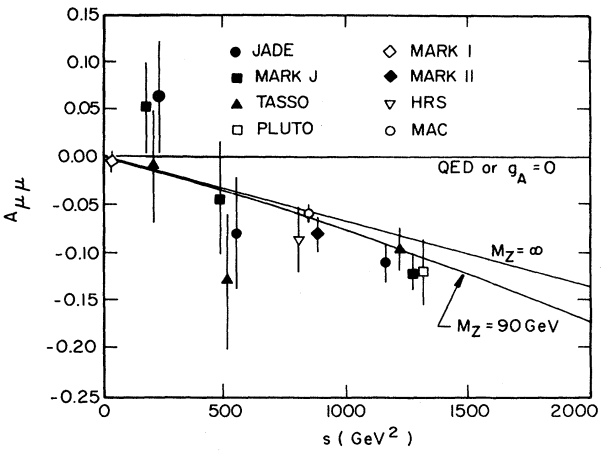

FIG. 12. Muon-pair forward-backward charge asymmetry.

$A_{\mu\mu}=-0.084\pm0.043$. The full sample of muon pairs yields a raw asymmetry $A_{\text{raw}}=-0.046\pm0.035$. Over this limited solid angle the Monte Carlo calculation yields an asymmetry from α^3 QED of $A_{\text{QED}}=+0.012$. The effects of α^3 QED and detector acceptance are included in the distribution functions $P(g_A,\cos\theta)$ used to perform the fits. The data are thus corrected for such effects as part of the fitting procedure. The asymmetry $A_{\mu\mu}$ is due purely to the axial-vector coupling of the weak neutral boson.

Figure 12 summarizes the asymmetry measurements of this and other experiments.[13] The prediction of the electroweak theory is indicated by the smooth curves. The angular distribution of the radiatively corrected muon-pair data is shown in Fig. 13. The curve includes lowest-order QED plus weak interactions with the couplings determined by the fit ($g_A{}^2=0.33$).

The angular distributions imply limits on nonstandard unified models containing two neutral weak bosons.[14] The masses of the pair of bosons are related to the weak mixing angle through a parameter C which modifies the vector coupling $g_V{}^2\to(1-4\sin^2\theta_W)^2+16C$. For $\sin^2\theta_W=0.23$ we find that $C<0.038$ at the 95% confidence level. We have

$$C=\gamma\frac{(M_2{}^2-M_Z{}^2)(M_Z{}^2-M_1{}^2)}{M_1{}^2M_2{}^2}$$

where $\gamma=\sin^4\theta_W$ or $\gamma=\cos^4\theta_W$ for the models based on $SU(2)\times U(1)\times SU(2)'$ and $SU(2)\times U(1)\times U(1)'$, respectively. When $\gamma=\sin^4\theta_W$, $M_1>40$ GeV when $M_2>29$ GeV. As M_2 increases so does the lower limit for M_1. For $\gamma=\cos^4\theta_W$, $M_1>80$ GeV for $M_2>29$ GeV. The measurement of a negative asymmetry implies that the mass of any weak neutral boson is greater than 29 GeV at the 95% confidence level. The lower limits for a second massive neutral boson in the two nonstandard models are thus 40 and 80 GeV.

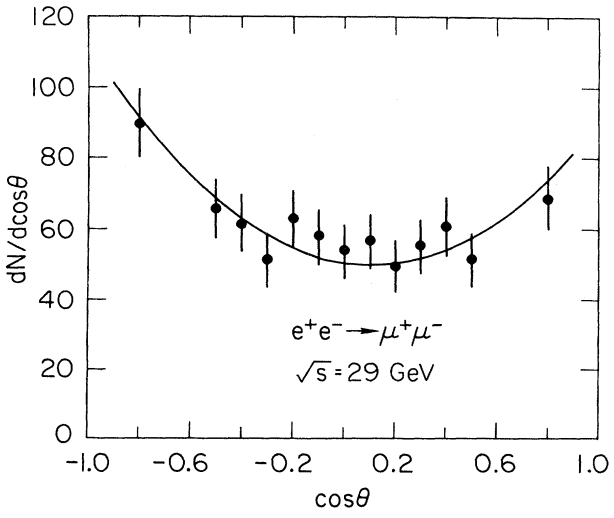

FIG. 13. The angular distribution of muons.

VI. SEARCH FOR SCALAR-ELECTRON PAIR PRODUCTION (REF. 15)

A. Introduction

Because of the great success of the unified gauge theory of electromagnetism and the weak force, it is natural to attempt a further unification to include quantum chromodynamics. Incorporating quantum chromodynamics leads to grand unified theories (GUT's) of particle interactions. There are many models of GUT, each having its own predictions. One attractive model is supersymmetry,[16] in which all particles are placed in supermultiplets which include both fermions and bosons in the same multiplet.

The model that we consider is the lowest dimension, $N=1$ model,[17] which calls for only one set of bosons and fermions to be related by supersymmetry into a supermultiplet. A chiral multiplet consists of a spin-half fermion of definite chirality, for example, $\tilde{e}_L$, with two degrees of freedom. The normal Dirac electron, with components e_L,e_R, then has two scalar field components $\tilde{e}_L,\tilde{e}_R$ associated with it, representing a pair of physical particles. These partners of the electron have identical quantum

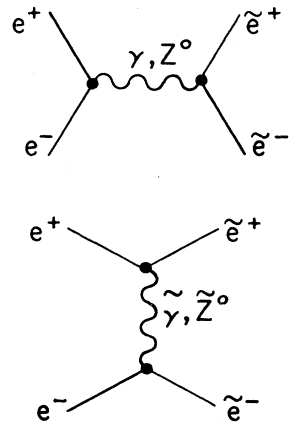

FIG. 14. Scalar-electron pair production in the s channel and t channel.

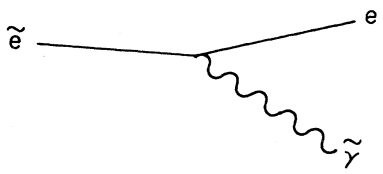

FIG. 15. Scalar-electron decay into a photino and an electron.

numbers except for spin, and, in the limit of exact supersymmetry, are degenerate in mass. At what scale and, in fact, how the supersymmetry breaks the symmetry is model dependent, and hence so are the masses of the partners.

It is assumed that the partner to the photon, the spin-$\frac{1}{2}$ photino, has a small or vanishing mass which is much less than $M_{\tilde{e}}$. The lowest-energy supersymmetric-particle production is then shown in Fig. 14 and consists of the production of a pair of scalar electrons through both an s-channel and a t-channel graph. The scalar electron has the same coupling to the photon as do normal leptons, but because the scalar electron carries the electron quantum number, there is the additional process involving the exchange of a photino. The cross section is then given by[18]

$$\frac{d\sigma(e^+e^-\to\tilde{e}^+\tilde{e}^-)}{d(\cos\theta)} = \frac{\pi\alpha^2\beta^3\sin^2\theta}{4s}\left[1+\left[1-\frac{4K}{1-2\beta\cos\theta+\beta^2}\right]^2\right],$$

where $K=1$ for scalar electron and $K=0$ for scalar muons (no t channel). The spin-0 electrons then decay with a very short lifetime to a normal spin-$\frac{1}{2}$ electron plus a photino as shown in Fig. 15. The photino is expected to be a neutrinolike object that leaves the interaction region undetected. The final state expected in the detector is then two noncoplanar electrons with a large amount of missing energy. Thus, we search for the reaction

$$e^+e^-\to\tilde{e}^+\tilde{e}^- \to e^-\tilde{\gamma}\ ,\quad e^+\tilde{\gamma}\ .$$

B. Monte Carlo simulation

In order to understand how the experimental cuts necessary to remove backgrounds affect a possible scalar-electron signal, a Monte Carlo simulation was done. The generator produced a pair of spin-0 charged particles with the correct differential distribution including both virtual and hard radiative effects. The calculations used for the radiative effects are those of Berends and Kleiss[19] which included the effects of leptonic and hadronic vacuum polarization as well as initial- and final-state radiation. A radiative photon was considered detectable if its energy was greater than 100 MeV.

The final-state electron, positron, and photon were then passed through a realistic model of the spectrometer as described earlier. Similarly, the Bhabha scattering and τ-lepton production were modeled in order to understand the effects of such backgrounds to a possible scalar-electron signal.

C. Event selection

A sample of events with two electrons in the final state was selected from the initial 16×10^6 triggers by demanding that the event contain only two oppositely charged tracks, each with a momentum greater than 1 GeV/c and pass within a radial distance of 10 cm of the beam axis and be less than ±15 cm from the interaction point along the beam line. Each track was also required to have an associated barrel shower hit with an energy deposition of at least 30% of its momentum to identify it as an electron. A time-of-flight difference between the two tracks of less than 8 nsec was required to eliminate cosmic rays. The data sample then consisted of 12 065 events, almost identical to that used in the analysis of Bhabha events.

The production of scalar electrons and the subsequent decay of each to an electron and a photino results in a four-body state, with two of the particles not observed. The observed final state would then consist of two noncoplanar electrons with, on average, only half of the total center-of-mass energy. Figure 16 shows the calculated total visible energy and acoplanarity distributions for scalar-electron masses of 2.0 and 11.0 GeV/c^2, respectively. To eliminate nonradiative Bhabha events, it was required that the sum of the momenta of the two electrons be less than 95% of the total electron center-of-mass energy. In addition, it was required that the total electron energy be greater than 20% of $E_{\text{c.m.}}$; this cut vetoed against possible two-photon ($e^+e^-\to e^+e^-e^+e^-$) contamination.

The major background comes from the three-body radiative Bhabha events. These events must be coplanar to conserve momentum and this difference from the scalar-electron signal is used to substantially reduce the Bhabha contribution. Because no attempt has been made to mea-

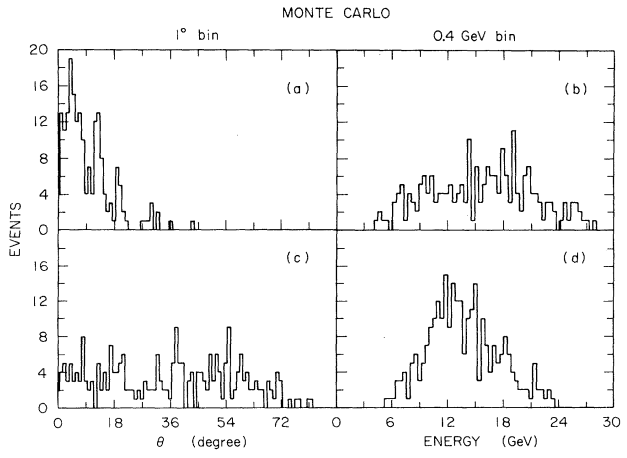

FIG. 16. The calculated scalar-electron (a) acoplanarity distribution for mass 2 GeV/c^2, (b) total visible energy for mass 2 GeV/c^2, (c) acoplanarity distribution for mass 11 GeV/c^2, and (d) total visible energy for mass 11 GeV/c^2.

sure the photon direction at this stage, the plane of the event with respect to which the transverse momentum is conserved cannot be defined. Instead, we define an acoplanarity angle by using the normalized momentum vectors $\hat{p}_{e+}$ and $\hat{p}_{e-}$ of the final-state electrons and $\hat{z}$, the beam axis.

$$\cos(\chi)=(\hat{p}_{e+}\times\hat{z})\cdot\hat{p}_{e-}\ ,$$

$$\theta_{\text{acop}}=\left|\frac{\pi}{2}-\chi\right|\ .$$

This parameter has the qualitative features of the "true" acoplanarity of the event; that is, it is very strongly peaked for those events that are expected to be coplanar and very much less so for those which are not. A comparison of the calculated scalar-electron decay distributions in Fig. 16 with that for Bhabha scattering in Fig. 17 shows that there is a very good rejection of the background-to-signal for the high-mass scalar electrons, but that the distributions become very similar for the low-mass case. This is due to the kinematics of low-mass particle production which tends to give a large boost to the decay products along the production direction. Because the scalar electrons are produced back-to-back the final states tend to be collinear.

A minimum acoplanarity angle of 25° was found to be optimum for reducing the background for scalar-electron masses down to that of the τ lepton at 1.78 GeV/c^2. Extending the scalar-electron mass to lower values causes a large increase in the background from τ pair production. The acoplanarity cut at 25° reduced the sample to 81 events. These events were handscanned for anomalous features. None were found.

Up to this point events have been selected with two charged tracks regardless of whether or not neutral particles had been identified by the shower-counter system. This was done to check the consistency of the event sample distributions with those of QED. If it is now required

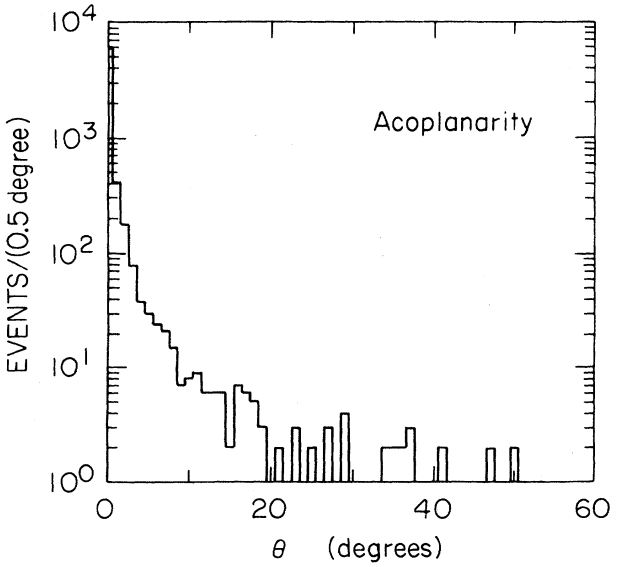

FIG. 17. Measured acoplanarity for Bhabha scattering.

that there be no hard photons with $E_\gamma \geq 400$ MeV anywhere in the shower system, we are left with a sample of six events. This cut causes a slight reduction in the scalar-electron signal because of the initial-state radiation, correctly modeled into the Monte Carlo. However, the Bhabha background is now strongly excluded because events that survived the acoplanarity cuts had to have an associated hard photon. Only those Bhabha events with large acoplanarity and having an associated hard photon entering a gap or crack in the shower-system coverage were accepted.

The prediction, after passing the Bhabha Monte Carlo events through the detector-simulation program, is that 4.8 Bhabha events are expected in the measured data sample. Similarly, the τ Monte Carlo predicts that less than 0.02 τ events should be expected in this sample.

After carefully hand-scanning these six remaining candidate events, four are found to be clear α^3 radiative Bhabha events in which the photon hit near one of the electrons in the shower-counter system or else it passed through a shower-counter crack so that less than 10% of its energy was observed. The probability of a random or noise hit in a shower-counter module has been measured to be less than 0.25%, meaning that in the sample of six events, the expectation of a random or nonevent associated shower-counter hit is less than 0.5. For each of these events the electron and positron momenta were used to calculate the missing momentum and in each case the observed energy deposition matched the predicted location. It should be noted that these effects have been modeled into the Monte Carlo simulation of scalar-electron production and are included in the calculation of the expected number of events.

The remaining two events are inconsistent with being simple α^3 radiative Bhabha events. One event has two well separated shower-module hits and is consistent with an α^4 radiative Bhabha event in which both photons, one of 10 GeV and the other of 6 GeV, fell into cracks that make up about 10% of the barrel shower-counter system. The magnitude of the missing energy yields both photon energies. Using these values along with the observed locations of the hits in the shower modules give an event that satisfies conservation of momentum for each component of the momentum.

D. Result of search

The last event, shown in Fig. 18, has no additional barrel shower-counter hits. Accordingly, it is inconsistent with having a single missing photon because the missing energy is larger than the beam energy of 14.5 GeV. It is consistent with $e^+e^-\rightarrow e^+e^-\gamma\gamma$ in which both radiated photons fall in the 1-sr gap between the barrel and endcap shower-counter systems. Although there are presently no reliable event generators which model α^4 QED, crude estimations of the expected number of these events in this sample is of order 1.

This event, then, is consistent with being an $ee\gamma\gamma$ final state. But because the photons have not been detected, it cannot be excluded as a candidate for scalar-electron production. For the supersymmetric model and the selection criteria stated, this event cannot be uniquely assigned to

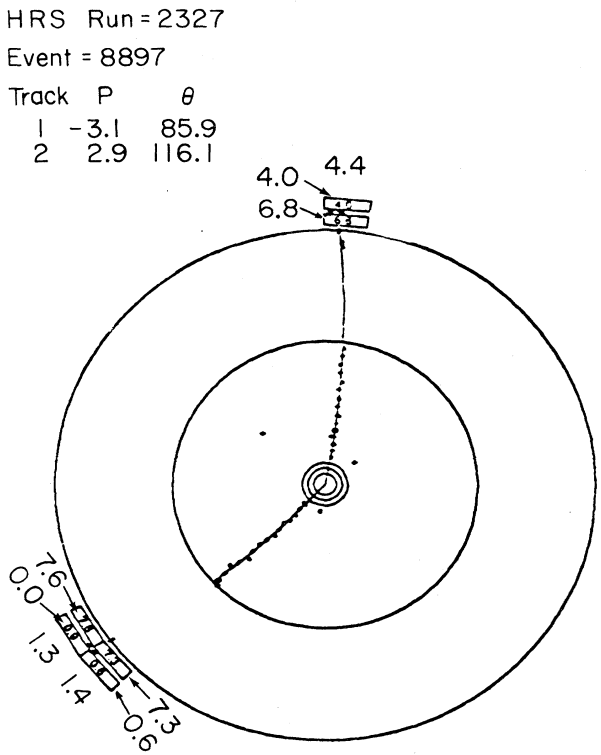

FIG. 18. Candidate scalar-electron event consistent with QED production; values shown (closest to interaction region first) are uncorrected values of time of flight, energy deposition in three radiation lengths, and total energy deposition.

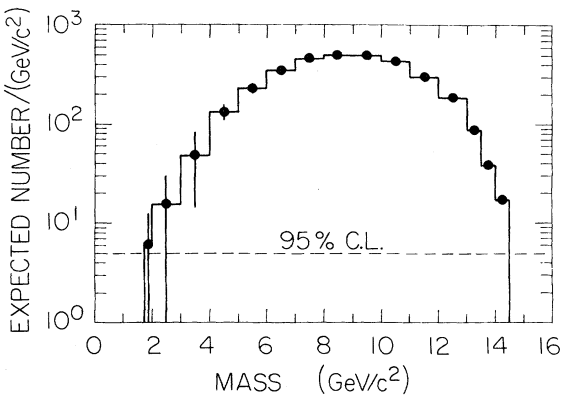

FIG. 19. Scalar-electron mass limits.

only one category due to the limited acceptance of the detector. Hence, this single event represents the limit of sensitivity for this analysis and it is used to determine the the excluded mass range for scalar-electron production.

With a final event sample of one, the 95%-confidence-level limit is five events. Figure 19 shows the Monte Carlo calculation for the expected number of scalar-electron events. The dropoff at the low-mass values is due to the analysis cuts. The dropoff at the high mass values is due to the β^3 cutoff in the cross section. From this calculation we find that the mass of the supersymmetric partner of the electron is excluded to a 95% confidence level in the range $1.8 < M_{\text{scalar}} < 14.2$ GeV/c^2.

In conclusion, we have measured Bhabha scattering and muon pair production based on an exposure of the HRS to the 29-GeV center-of-mass energy e^+e^- colliding beams at PEP. The results agree well with the predictions of quantum electrodynamics and the standard model of weak interactions. We have found that these theories are in excellent agreement with the data. We have also compared our results to extensions of the standard model and find no evidence in support of these proposed extensions.

ACKNOWLEDGMENTS

This work was supported by the United States Department of Energy and one of the authors (R.T.) was supported in part by the Sloan Foundation. The experiment was made possible by the excellent support provided by the technical staffs of the collaborating institutions. We also wish to thank the PEP staff who were responsible for the operation of the storage ring.

*On leave of absence from Istituto Nazionale di Fisica Nucleare, Pisa, Italy.

[1]S. L. Glashow, Nucl. Phys. **22**, 579 (1962); A. Salam, Phys. Rev. **127**, 331 (1962); S. Weinberg, Phys. Rev. Lett. **19**, 1264 (1967); S. L. Glashow, A. Salam, and S. Weinberg, Rev. Mod. Phys. **52**, 515 (1980).

[2]The hadronic vacuum polarization contribution is non-negligible to the leptonic cross sections. Its effects are not predicted by the standard model but are determined empirically.

[3]D. Rubin *et al.*, Nucl. Instrum. Methods **203**, 119 (1982).

[4]G. Baranko *et al.*, Nucl. Instrum. Methods **169**, 413 (1980).

[5]R. L. Ford and W. R. Nelson, Report No. SLAC-210, 1978.

[6]R. Kleiss, Ph.D. thesis, University of Leiden, 1982; F. A. Berends, R. Kleiss, and S. Jadach, Nucl. Phys. **B202**, 63 (1982).

[7]D. Rubin, Ph.D. thesis, University of Michigan, 1983.

[8]F. A. Berends and G. J. Komen, Phys. Lett. **63B**, 432 (1979); F. A. Berends *et al.*, Nucl. Phys. **B68**, 541 (1974); F. A. Berends and R. Kleiss, *ibid.* **B117**, 237 (1981).

[9]R. Gatto, in *Proceedings of the International Symposium on Electron and Photon Interactions at High Energies, Hamburg, 1963* (Springer, Berlin, 1965), Vol. I, p. 106; S. D. Drell, Ann. Phys. (N.Y.) **4**, 75 (1978); T. D. Lee and G. Wick, Phys. Rev. D **2**, 1033 (1970); N. M. Kroll, Nuovo Cimento **XLV**, 65 (1966).

[10]E. Eichten, K. Lane, and M. Peskin, Report No. Fermilab-Pub-83/15-THY, 1983 (unpublished).

[11]F. A. Berends *et al.*, Nucl. Phys. **B202**, 63 (1982).

[12]Particle Data Group, M. Roos, *et al.*, Phys. Lett. **111B**, 26 (1982).

[13]JADE, W. Bartel, *et al.*, Z. Phys. C **19**, 197 (1983); Phys. Lett.

108B, 140 (1982); MARK J, Report No. MIT-LNS 124, 1982 (unpublished); D. P. Barber *et al.*, Phys. Lett. **95B**, 149 (1980); TASSO, M. Althoff *et al.*, DESY Report No. 83-089, 1983 (unpublished); PLUTO, Ch. Berger *et al.*, Z. Phys. C **21**, 53 (1983); MARK II, M. R. Levi *et al.*, Phys. Rev. Lett. **51**, 1941 (1983); MAC, E. Fernandez *et al.*, *ibid.* **50**, 1238 (1983); Report No. SLAC-Pub-3133, 1983 (unpublished). Also see B. Naroska, in *Proceedings of the 1983 International Symposium on Lepton and Photon Interactions at High Energies, Ithaca, New York,* edited by D. G. Cassel and D. L. Kreinick (Cornell University, Ithaca, 1983).

[14]V. Barger, W. Y. Keung, and E. Ma, Phys. Rev. Lett. **44**, 1169 (1980); E. H. de Groot *et al.*, Phys. Lett. **90B**, 427 (1980).

[15]R. J. Wilson, Ph.D. thesis, Purdue University, 1983.

[16]H. Georgi and A. Pais, Phys. Rev. D **10**, 539 (1974).

[17]J. Wess and B. Zumino, Phys. Lett. **49B**, 52 (1974).

[18]I. Hinchliffe and L. Littenberg, in *Proceedings of the 1982 DPF Summer Study on Elementary Particle Physics and Future Facilities, Snowmass, Colorado,* edited by R. Donaldson, R. Gustafson, and F. Paige (Fermilab, Batavia, Illinois, 1982); G. R. Farrar and P. Fayet, Phys. Lett. **89B**, 191 (1981).

[19]F. Berends and R. Kleiss, Nucl. Phys. **B178**, 141 (1981).